The Impact of Functionalization on the Stability, Work Function, and Photoluminescence of Reduced Graphene Oxide

Priyank V. Kumar, Marco Bernardi, and Jeffrey C. Grossman*

Department of Materials Science and Engineering, Massachusetts Institute of Technology, 77 Massachusetts Avenue, Cambridge Massachusetts 02139-4307, United States

ABSTRACT Reduced graphene oxide (rGO) is a promising material for a variety of thin-film optoelectronic applications. Two main barriers to its widespread use are the lack of (1) fabrication protocols leading to tailored functionalization of the graphene sheet with oxygen-containing chemical groups, and (2) understanding of the impact of such functional groups on the stability and on the optical and electronic properties of rGO. We carry out classical molecular dynamics and density functional theory calculations on a large set of realistic rGO structures to decompose the effects of different functional groups on the stability, work function, and photoluminescence. Our calculations indicate the metastable nature of carbonyl-rich rGO and its favorable transformation to hydroxyl-rich rGO at room temperature *via* carbonyl-to-hydroxyl conversion reactions near carbon vacancies and holes. We demonstrate a significant tunability in the work function of rGO up to 2.5 eV by altering the composition of oxygen-containing functional groups for a fixed oxygen concentration, and of the photoluminescence emission by modulating the fraction of epoxy and carbonyl groups. Taken together, our results guide the application of tailored rGO structures in devices for optoelectronics and renewable energy.

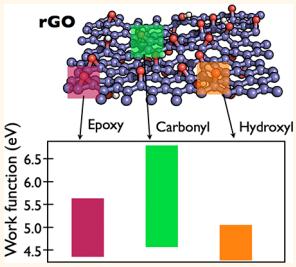

KEYWORDS: reduced graphene oxide · molecular dynamics · density functional theory · work function · stability · photoluminescence · functional groups

Reduced graphene oxide (rGO) is emerging as a solution-processable material for a large number of applications including ultrathin flexible electronics,[1−5] sensors,[6] catalysis,[7−9] composites,[10−13] and energy conversion and storage technologies.[14−17] rGO consists of a one-atom thick layer of graphene decorated with oxygen-containing functional groups such as carbonyl, hydroxyl, epoxy, and ether groups. The possibility of varying the concentration of such chemical groups and their relative position on the graphene sheet makes rGO a highly versatile functional material. For example, the optical absorption and photoluminescence (PL) can be tuned in the visible, and the carrier mobility can be varied over 9−12 orders of magnitude by altering the ratios of various functional groups and of sp^2/sp^3-hybridized carbon atoms.[18−20] Despite the presence of such a vast design space for rGO, fabrication protocols capable of tailoring the proportion of different functional groups and their positioning on the graphene sheet are still lacking,[2,21] as is a detailed understanding of the impact of each type of functional group on key properties for applications in optoelectronics, such as the work function and photoluminescence (PL).

Another barrier toward the technological application of rGO is the control of structural and chemical transformation processes with the potential to alter functionality over time. Different chemical groups on the rGO sheet are inter-related by a complex network of interconversion reactions, thus limiting the stability of rGO and its reliability as a functional material. It is therefore of central importance to understand structure−property relations in rGO with atomistic detail, and to shed light on the effects of key functional groups present in rGO.[22,23] While experimental characterization of rGO at the molecular scale is a challenging task because of its disordered and chemically heterogeneous nature, atomistic simulations of rGO[24−28] can be employed to achieve an in-depth understanding of the main trends in structure−property relations.

* Address correspondence to jcg@mit.edu.

Received for review November 27, 2012 and accepted January 23, 2013.

Published online January 31, 2013
10.1021/nn305507p

© 2013 American Chemical Society

In this work, we employ atomistic simulations using classical molecular dynamics (MD) and *ab initio* density functional theory (DFT) methods to study a large statistical set of rGO structures with a range of chemical compositions and displaying realistic disorder in the positioning of the functional groups. We adopt a reduction protocol based on classical MD simulations with reactive force fields to generate over 360 rGO structures (each with over 200 atoms in the simulation cell) starting from nine different graphene oxide (GO) compositions (see Methods). We apply DFT calculations to this large set of structures in order to study reaction paths limiting the kinetic stability of as-prepared rGO, as well as to correlate structural features in the rGO sheet with trends in the work function, electronic structure, and PL. We demonstrate that it is possible to decouple the impact of individual functional groups such as epoxy, hydroxyl, and carbonyl on each of these properties, and show how the controlled modulation of specific functional groups can be used to fine-tune the functionality of rGO, including achieving variations of up to 2.5 eV in the work function and significant shifts in the frequency of peak PL emission. Our calculations further reveal the metastable nature of a common form of as-synthesized rGO (carbonyl-rich rGO), and indicate possible atomistic mechanisms for its spontaneous conversion to the energetically more favorable hydroxyl-rich rGO with lower defect concentration. Taken together, our results define several structure–property relations in rGO and guide the preparation of tailored rGO structures for application in optoelectronics and renewable energy.

RESULTS AND DISCUSSION

Figure 1a shows our computational synthesis protocol for generating rGO structures using MD simulations. Initial GO structures consist of randomly distributed epoxy and hydroxyl groups attached to both sides of the graphene sheet, consistent with previous work showing the dominant presence of such functional groups in GO.[23,24,29] We employ different oxygen concentrations (in atom % hereafter) of 15%, 20%, and 25% in the initial GO structures,[24] and prepare samples with epoxy to hydroxyl ratios of 3:2 and 2:3. GO preparation is followed by thermal reduction of GO structures at 1500 K using classical MD simulations, and structural relaxation and characterization using DFT (Figure 1a and Methods).

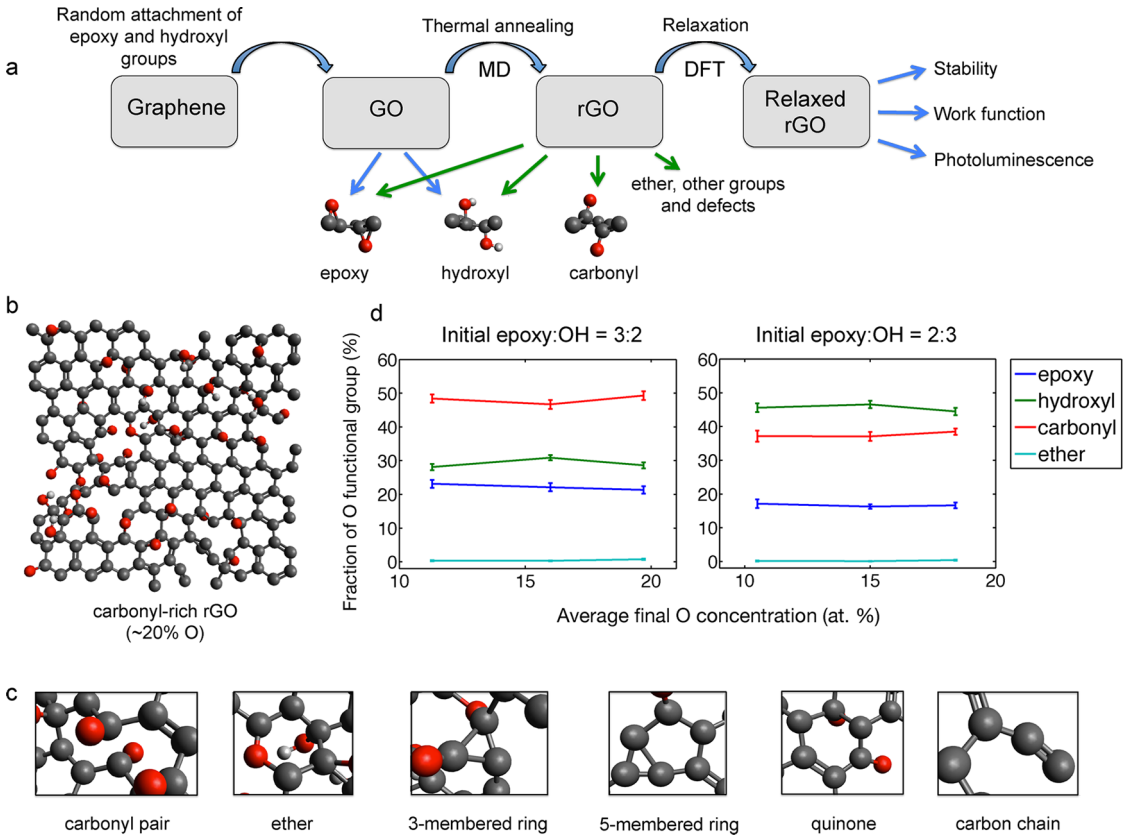

Figure 1. (a) Schematic of the preparation protocol of rGO. (b) Representative disordered carbonyl-rich rGO structure. Carbon, oxygen, and hydrogen are represented as gray, red, and white spheres, respectively. (c) Various groups and defects formed during high temperature reduction of GO by conversion of initial epoxy and hydroxyl groups. (d) Average fraction of oxygen-containing functional groups as a function of average final oxygen concentration in the rGO sheets, for different initial GO structures with epoxy to hydroxyl ratios of 3:2 (left) and 2:3 (right). The thermal reduction of these two cases results in, respectively, carbonyl-rich rGO (left) and hydroxyl-rich rGO (right). In each plot, the results are obtained by averaging over 40 rGO structures, and the error shown represents the standard error of the mean calculated for the same set of structures.

Our thermal reduction simulations lead to the formation of disordered rGO structures with a range of functional groups, such as epoxy and hydroxyl groups initially present in rGO, carbonyl and ether groups, three- and five-membered carbon rings, quinones, and carbon chains (Figure 1b,c), consistent with previous computational work.[24] The generation of a large number of structures allows us to establish statistically meaningful averages for the relative distribution of functional groups present in rGO after the reduction process. Figure 1d shows a key trend we observe in our simulations, namely that thermal reduction of epoxy-rich GO (initial epoxy to hydroxyl ratio of 3:2) results in carbonyl-rich rGO structures, whereas thermal reduction of hydroxyl-rich GO (initial epoxy to hydroxyl ratio of 2:3) results in hydroxyl-rich rGO structures. Additional reduction data is available in the Supporting Information.

Next, we employ DFT calculations to study the kinetic stability of the generated rGO structures, by computing their formation energy as a function of oxygen and hydrogen chemical potentials (or equivalently, partial pressures) as:

$$E_{form} = E_{tot}(C_lO_mH_n) - lE(C_{gr}) - m\mu_O - n\mu_H$$

where $E_{tot}(C_lO_mH_n)$ is the total energy of the rGO structure with l carbon, m oxygen, and n hydrogen atoms, $E(C_{gr})$ is the energy of a carbon atom in a pristine graphene,[28] and the reference chemical potentials of oxygen (μ_O) and hydrogen (μ_H) are chosen as those in O_2 and H_2 gas molecules, respectively.[28,30]

The computed trends for the formation energies of carbonyl-rich and hydroxyl-rich rGO (Figure 2a) suggest that hydroxyl-rich rGO with low oxygen content is favorable over a wide range of oxygen partial pressures. Conversely, the formation of carbonyl-rich structures with higher oxygen content is favorable only at high oxygen partial pressures. On this basis, we suggest that while as-synthesized rGO commonly displays large fractions of oxygen-rich epoxy and carbonyl groups,[24,31,32] such rGO structures are only kinetically stable and may evolve to hydroxyl-rich structures with lower oxygen content once exposed to lower temperatures and oxygen partial pressures than those used during the reduction process. Our predictions are corroborated by recent experimental work from Kim *et al.*,[33] where as-synthesized multilayer GO films rich in epoxy groups evolved toward hydroxyl-rich GO at room temperature. A key mechanism involved in this spontaneous reduction of rGO is water formation *via* the interaction of hydrogen and oxygen atoms within the basal plane, a process observed to be favorable at room temperature and under ambient atmospheric hydrogen and oxygen partial pressures (see Figure 2a).

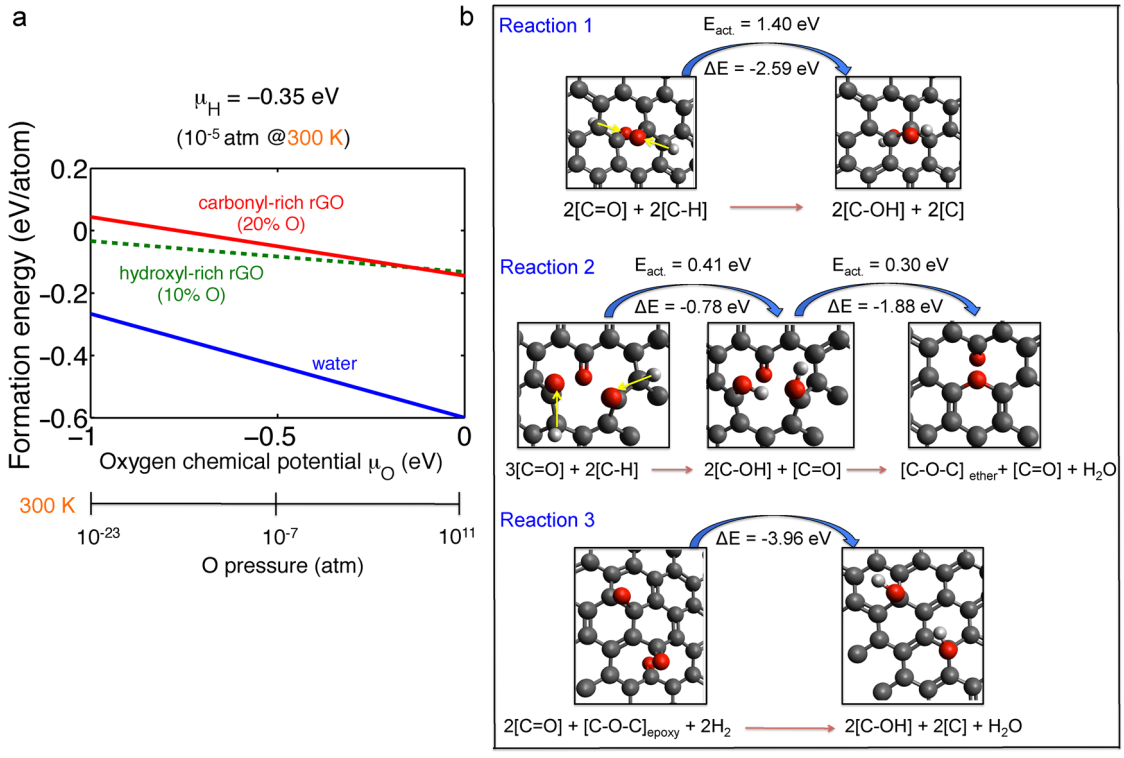

Figure 2. Stability of as-prepared rGO structures. (a) Formation energy per atom of hydroxyl-rich (10% O) and carbonyl-rich (20% O) rGO structures as a function of oxygen chemical potential, shown for the standard value (−0.35 eV) of atmospheric hydrogen chemical potential at 300 K. The energetics shown in the plot indicates the higher stability of hydroxyl-rich rGO compared to carbonyl-rich rGO, and the tendency of both to undergo a reduction process *via* the elimination of water. (b) The three reaction mechanisms studied here for the conversion of carbonyl groups to hydroxyl groups in the presence of chemisorbed H atoms. Reactions 2 and 3 involve reduction *via* elimination of water, while reaction 1 does not involve water formation.

To elucidate the atomistic mechanisms involved in the reduction of carbonyl-rich to hydroxyl-rich rGO, we examined three possible reaction pathways (Figure 2b) capable of converting carbonyl to hydroxyl groups in rGO, and quantified the associated energetics using nudged elastic band calculations. Since carbonyl groups occur commonly in pairs or at the periphery of carbon vacancies in rGO, we consider two reaction schemes involving a carbonyl pair or a carbonyl-vacancy pair (respectively, Reaction 1 and 2 in Figure 2b). In addition, we investigate a third reaction scheme (Reaction 3 in Figure 2b) where the interaction of a carbonyl group with an epoxy group leads to rGO reduction, a case chosen to emphasize the importance of interplay between functional groups in the rGO sheet. In our proposed reaction schemes, hydrogen is assumed to be present in the chemisorbed form (within C−H bonds), as commonly generated during GO synthesis[33] or exposure to air. As a result, the three proposed reaction mechanisms are limited by the diffusion of C−H bonds across the basal plane (a process known to have an energy barrier of 0.55 eV[33]) and by the availability of H in the environment.

In the first reduction mechanism (Reaction 1 in Figure 2b), a carbonyl pair interacts with chemisorbed H and forms a hydroxyl pair, with an energy gain obtained from our DFT calculations of 2.59 eV. The second reduction mechanism (Reaction 2 in Figure 2b) is a two-step process: in the first step, carbonyl groups at the periphery of a carbon vacancy react with hydrogen to form hydroxyl groups, with a calculated energy gain of 0.78 eV. In the second step, the interaction between the so-formed hydroxyl groups leads to water formation and the elimination of a vacancy by forming an ether group, a process with an energy gain of 1.88 eV based on our calculations. In the last reaction scheme proposed here (Reaction 3 in Figure 2b), a carbonyl pair and an epoxy group interact to form two hydroxyl groups and a water molecule with a predicted energy gain of 3.96 eV. *Our calculations suggest that all mechanisms considered here are energetically favorable and are thus predicted to occur thermodynamically*; the computed energetics confirms the tendency of rGO to undergo further reduction and "self-heal" over time by restoring sp^2 carbon atoms in the graphene lattice.

We estimate the kinetics of Reactions 1−3 by computing their rates using the Arrhenius formula:

$$k = k_0 \exp(-E_{act}/kT)$$

where E_{act} is the activation energy computed using the nudged elastic band method (Figure 2b), and k_0 is an attempt frequency with an assumed value of 10^{13} hz. At room temperature (300 K), we predict Reactions 1 and 3 to possess a high activation energy of 1.40 eV limited by the process of "hole" closure in these cases, causing a slow reaction rate of $k \approx 10^{-11}$ hz. For comparison, the first step of Reaction 2 involving a chemical process similar to Reaction 1 (in terms of converting carbonyl to hydroxyl groups) but occurring near C vacancies is significantly faster, achieving an estimated carbonyl-to-hydroxyl conversion rate of 10^6 hz, and involving a significantly lower energy barrier of 0.41 eV. Our calculations suggest that the higher activation barrier for Reaction 1 is related to the presence of strain during the carbonyl pair reaction, while in Reaction 2 strain is reduced by the presence of a vacancy in the basal plane. The increased reduction rate found here near C vacancies is consistent with the recent experimental observation of spontaneous healing of nanoholes in graphene.[34] We conclude that although rGO obtained *via* thermal annealing is kinetically stable with a significant fraction of carbonyl groups,[24] these structures may evolve toward hydroxyl-rich rGO over time, as suggested by the calculations discussed above. The sensitivity of the optical and electronic properties on functional group composition discussed below implies that such important stability considerations should be carefully assessed before incorporating rGO into functional devices.

In what follows, we perform DFT calculations on the library of realistic rGO structures generated in this work, with the goal of studying the dependence of the electronic structure and work function of rGO on the concentration of different functional groups. In particular, we explore the impact of two crucial parameters on the work function: (1) the overall oxygen concentration, and (2) the concentration of different types of functional groups. The work function tunability in rGO stems from the formation of dipoles between carbon and oxygen atoms with different electronegativity. Oxygen atoms in carbonyl, epoxy, and hydroxyl groups are located outside the graphene basal plane, and form C−O bonds of different types and with different chemical surroundings. As a consequence, the strength of the out-of-plane dipole moment in rGO can be tuned by varying both the overall oxygen content and the concentration of different functional groups.

Figure 3a shows the work function computed for rGO structures prepared in this work, with oxygen concentration in the 10−20% range. Within this oxygen concentration range, the work function is found to be tunable between 5.0−5.5 eV, thus allowing a 0.5 eV variation within this range by adjusting the reduction conditions. We expect the tunability to increase further if a wider oxygen concentration range is considered.

In addition to this favorable effect, we demonstrate here that oxygen concentration is not the main variable controlling the work function, and that a significantly higher work function tunability spanning a range of 2.5 eV can be obtained by varying the fraction of a single type of functional group. To isolate the impact of different functional groups on the work function, we carried out DFT calculations on smaller structures (approximately 130 atoms) than considered

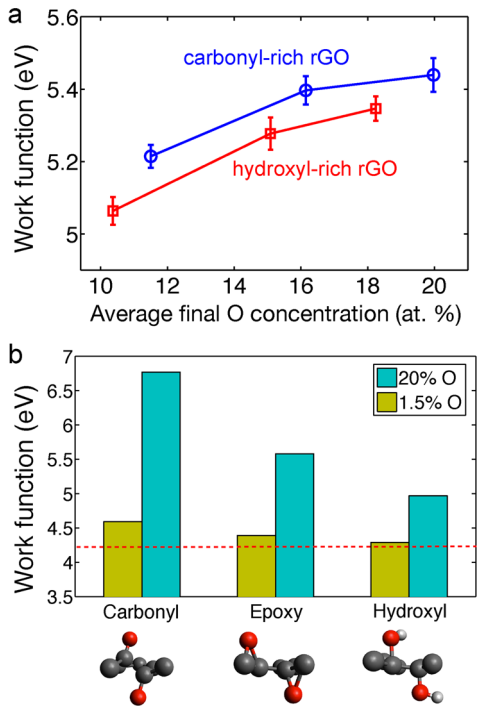

Figure 3. Work function tunability in rGO structures. (a) Calculated work function of carbonyl-rich and hydroxyl-rich rGO structures with different oxygen content. (b) The effect of individual functional groups on the work function of rGO, for two different total oxygen concentrations of 1.5% (for validation purpose) and of 20%. Carbonyl groups show the largest impact on the work function among all groups, inducing a work function value 60% higher than that of graphene (4.2 eV, shown here for reference as a dashed red line).

above, containing only one type of functional group—epoxy groups, hydroxyl groups, and carbonyl groups. In each case, we consider two values of the total oxygen concentration: 20%, considered here as an upper limit of oxygen concentration in rGO, and 1.5%, used here to assure that in the limit of a graphene structure with only one oxygen-containing functional group a work function value close to that of pristine graphene (4.2 eV) is obtained. For intermediate oxygen concentrations, the work function varies continuously within the range delimited by these two cases.

Figure 3b shows our calculated work function for structures with a single type of functional group. We observe the dominant effect of carbonyl groups, as seen by work function values in the 4.4−6.8 eV range for rGO structures containing only carbonyl groups. This represents a 60% increase compared to the computed work function of graphene (4.2 eV), an effect we attribute to the large dipole moment of the C−O double bond in carbonyl groups. We find a considerable impact on the work function also in the case of epoxy groups, yielding work function values in the 4.35−5.6 eV range, representing an increase by up to 32% compared to graphene. For hydroxyl groups, we observe a more moderate effect, yielding work function values in the 4.25−4.95 eV range, up to 17% higher than graphene. It is worth noting that in all cases considered, the work function is never lower than that of graphene, due to the orientation of the C−O dipoles pointing outward from the basal graphene plane in all cases considered. Our results explain recent experimental work showing a wide range of work function values in rGO,[35−37] which we interpret as a consequence of different content of functional groups resulting from different experimental reduction protocols used.

We conclude that in order to take full advantage of the wide range of achievable work functions in rGO, experimental reduction techniques yielding rGO with specific types of functional groups should be devised. Recently suggested routes toward synthesis with functional-group control include using hydrogen to adjust the proportion of carbonyl and hydroxyl groups,[24] dissociating oxygen molecules in ultrahigh vacuum to achieve selective epoxy functionalization,[38] or the use of local reduction methods with nanometer resolution.[2]

Similar to the work function, the PL emission spectrum of rGO shows significant tunability when the oxygen concentration and the ratios of different functional groups are varied.[18,19] PL spectra of rGO samples commonly show two prominent features: a broad emission peak centered around 500−600 nm (2−2.5 eV photon energy, denoted as I_{P1}) and a narrow peak centered around 450−475 nm (2.6−2.75 eV photon energy, denoted as I_{P2}).[19] The energy of the narrow I_{P2} peak is known to depend on the size of sp^2-hybridized graphene domains within the rGO matrix,[19] while the broad I_{P1} peak is thought to be determined by disorder-induced defect states. However, a clear understanding of the effect of different functional groups present in rGO is still missing, and structural models employed so far to account for the nature of the I_{P1} peak can only provide a qualitative picture of the role of disorder.[18,19,26]

We perform DFT electronic structure calculations on selected samples within our database of rGO structures, with the objective of elucidating the nature of the PL peaks in rGO at the atomistic level, and to decompose the contributions of different functional groups to the I_{P1} PL emission peak. Figure 4a shows the electronic structure of two carbonyl-rich rGO samples with respectively low (10%) and high (20%) total oxygen concentration, expressed in terms of the projected density of states (PDOS) from carbon atoms in the rGO structure. The carbon PDOS is chosen here as the main variable since in rGO the frequency and intensity of peak PL emission are governed by the π and π^* "tail" electronic bands, arising from carbon p_z states.

Figure 4a shows the presence of a significantly higher fraction of defect states around the Fermi energy (E_F) for the rGO sample with higher oxygen concentration, with the formation of a well-defined

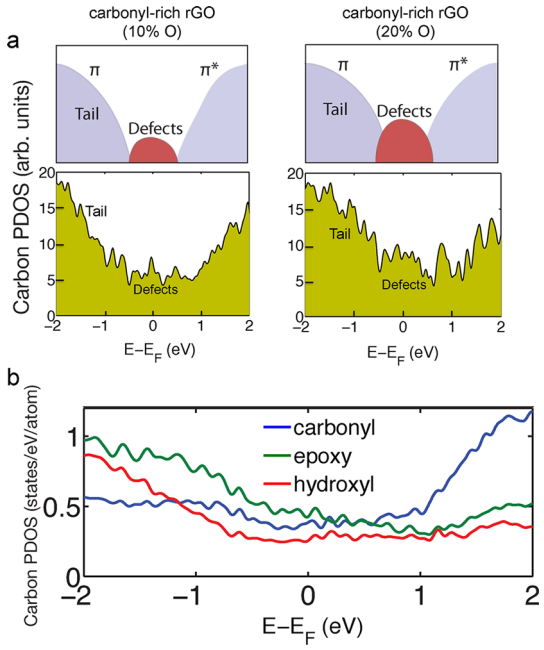

Figure 4. (a) Carbon PDOS plots for carbonyl-rich rGO with 10% (left) and 20% (right) oxygen concentrations. Above the plots, the contribution of defect and π–π* tail states to the PDOS is shown schematically for the two cases. (b) PDOS from carbon atoms in carbonyl, epoxy, and hydroxyl groups, shown here for 20% oxygen concentration. Similar trends are found for 10% oxygen concentration.

PDOS feature between the π and π* tail bands. We decouple the contribution of individual functional groups to the tail and defect states by computing the average PDOS arising from carbon atoms attached to different functional groups (Figure 4b). Our analysis shows that the valence band (π tail) states are localized mainly at epoxy groups, while the conduction band (π* tail) states are mostly contributed by carbonyl groups. On this basis, we suggest that it may be possible to control the π and π* tail bands by varying the ratio of epoxy and carbonyl groups. Assuming that the peak PL emission energy is set by the energy difference between the DOS peaks of the π and π* bands, a similar strategy of controlling the epoxy to carbonyl ratio could also allow one to tune the peak PL emission frequency. We note that an increase in the fraction of epoxy and carbonyl groups at the expense of hydroxyl groups causes a higher density of defect states, as seen by the higher PDOS values around E_F for epoxy and carbonyl groups compared to hydroxyl groups in Figure 4b. The possibility outlined here to combine distinct contributions from different functional groups to the PL is a unique feature of rGO, and will be the object of further investigation.

CONCLUSION

In summary, we decompose the contributions of individual functional groups to the stability, work function, electronic structure, and PL emission of rGO. Our results highlight the significant tunability of the optical and electronic properties of rGO, including variation of the work function by up to 2.5 eV in structures with a precise control of oxygen-containing functional groups, and significant changes in the DOS and related PL emission by changing the ratio of epoxy to carbonyl groups. Our calculations indicate the metastable nature at room temperature of carbonyl-rich rGO structures usually obtained in the experiment, and show the favorable energetics for their conversion to hydroxyl-rich structures with lower oxygen content, driven by the carbonyl to hydroxyl conversion near carbon vacancies and holes. Our computational approach provides the basis to simulate realistic rGO structures, and our results strongly suggest that further efforts are necessary in controlling the content of individual functional groups in rGO to fully take advantage of its outstanding potential for functional devices.

METHODS

MD simulations used to prepare the rGO structures were carried out using the LAMMPS package[39] with the ReaxFF reactive force-field, chosen here for its ability to accurately describe bond-breaking and formation events in hydrocarbon systems.[40] We employed a time step of 0.25 fs and the NVT Berendsen thermostat.[24] Initial GO structures consisted of a 2.2 × 2.1 nm periodic graphene sheet containing 180 C atoms with randomly distributed epoxy and hydroxyl groups on both sides of the sheet.[41] During the reduction process, the temperature of the GO sheets was increased from 10 to 1500 K over a time interval of 250 fs. The system was then annealed at 1500 K for 250 ps to allow for structural stabilization. Molecular by-products released from the GO sheet were removed and the system was further annealed at 300 K for an additional 1.25 ps to confirm its stability. rGO structures generated with this approach were further relaxed (to less than 0.03 eV/Å residual atomic forces) using DFT with a plane-wave basis set as implemented in the VASP package.[42,43] In all the DFT calculations presented in this work, we used the Projector Augmented Wave (PAW) method to describe the core electrons[44] and the Perdew–Burke–Ernzerhof exchange-correlation (XC) functional[45] in combination with a gamma-point $\vec{k}$-grid. The wave function and charge density were expanded in plane waves with a wave function kinetic energy cutoff of 500 eV. A vacuum region of 16 Å was used in the direction normal to the sheets. For the study of reaction paths and energy barriers used to determine the kinetic stability of rGO, we employed nudged elastic band (NEB) calculations as implemented in VASP with 9–13 image structures between the reactant and the product.

Conflict of Interest: The authors declare no competing financial interest.

Acknowledgment. The authors acknowledge financial support from the Solar Frontiers Program at MIT. We thank NERSC and Teragrid for providing computational resources.

Supporting Information Available: Atomic coordinates of carbonyl-rich and hydroxyl-rich disordered rGO structures (files in the *xyz* format). Additional details of MD simulations. This material is available free of charge *via* the Internet at http://pubs.acs.org/.

Note Added after ASAP Publication: The version of this paper that was published ASAP on January 31, 2013, was missing the Supporting Information zip file containing the data files mentioned in the paragraph above. The files were correctly posted on February 14, 2013.

REFERENCES AND NOTES

1. Eda, G.; Fanchini, G.; Chhowalla, M. Large-Area Ultrathin Films of Reduced Graphene Oxide as a Transparent and Flexible Electronic Material. *Nat. Nanotechnol.* **2008**, *3*, 270–274.
2. Wei, Z.; Wang, D.; Kim, S.; Kim, S. Y.; Hu, Y.; Yakes, M. K.; Laracuente, A. R.; Dai, Z.; Marder, S. R.; Berger, C.; *et al.* Nanoscale Tunable Reduction of Graphene Oxide for Graphene Electronics. *Science* **2010**, *328*, 1373–1376.
3. Wobkenberg, P. H.; Eda, G.; Leem, D.-S.; De Mello, J. C.; Bradley, D. D. C.; Chhowalla, M.; Anthopoulos, T. D. Reduced Graphene Oxide Electrodes for Large Area Organic Electronics. *Adv. Mater.* **2011**, *23*, 1558–1562.
4. Stankovich, S.; Dikin, D. A.; Dommett, G. H. B.; Kohlhaas, K. M.; Zimney, E. J.; Stach, E. A.; Piner, R. D.; Nguyen, S. T.; Ruoff, R. S. Graphene-Based Composite Materials. *Nature* **2006**, *442*, 282–286.
5. Stankovich, S.; Dikin, D.; Piner, R.; Kohlhaas, K.; Kleinhammes, A.; Jia, Y.; Wu, Y.; Nguyen, S.; Ruoff, R. Synthesis of Graphene-Based Nanosheets *via* Chemical Reduction of Exfoliated Graphite Oxide. *Carbon* **2007**, *45*, 1558–1565.
6. Robinson, J. T.; Perkins, F. K.; Snow, E. S.; Wei, Z.; Sheehan, P. E. Reduced Graphene Oxide Molecular Sensors. *Nano Lett.* **2008**, *8*, 3137–3140.
7. Dreyer, D. R.; Jia, H.-P.; Bielawski, C. W. Graphene Oxide: A Convenient Carbocatalyst for Facilitating Oxidation and Hydration Reactions. *Angew. Chem., Int. Ed.* **2010**, *49*, 6813–6816.
8. Pyun, J. Graphene Oxide as Catalyst: Application of Carbon Materials Beyond Nanotechnology. *Angew. Chem., Int. Ed.* **2011**, *50*, 46–48.
9. Gao, Y.; Ma, D.; Wang, C.; Guan, J.; Bao, X. Reduced Graphene Oxide as a Catalyst for Hydrogenation of Nitrobenzene at Room Temperature. *Chem. Commun.* **2011**, *47*, 2432–2434.
10. Ramanathan, T.; Abdala, A. A.; Stankovich, S.; Dikin, D. A.; Herrera-Alonso, M.; Piner, R. D.; Adamson, D. H.; Schniepp, H. C.; Chen, X.; Ruoff, R. S.; *et al.* Functionalized Graphene Sheets for Polymer Nanocomposites. *Nat. Nanotechnol.* **2008**, *3*, 327–331.
11. Potts, J. R.; Dreyer, D. R.; Bielawski, C. W.; Ruoff, R. S. Graphene-Based Polymer Nanocomposites. *Polymer* **2011**, *52*, 5–25.
12. Kamat, P. V. Graphene-Based Nanoarchitectures. Anchoring Semiconductor and Metal Nanoparticles on a Two-Dimensional Carbon Support. *J. Phys. Chem. Lett.* **2010**, *1*, 520–527.
13. Lin, Y.; Zhang, K.; Chen, W.; Liu, Y.; Geng, Z.; Zeng, J.; Pan, N.; Yan, L.; Wang, X.; Hou, J. G. Dramatically Enhanced Photoresponse of Reduced Graphene Oxide with Linker-free Anchored CdSe Nanoparticles. *ACS Nano* **2010**, *4*, 3033–3038.
14. Xu, B.; Yue, S.; Sui, Z.; Zhang, X.; Hou, S.; Cao, G.; Yang, Y. What is the Choice for Supercapacitors: Graphene or Graphene Oxide? *Energy Environ. Sci.* **2011**, *4*, 2826–2830.
15. Kamat, P. V. Graphene-Based Nanoassemblies for Energy Conversion. *J. Phys. Chem. Lett.* **2011**, *2*, 242–251.
16. Murray, I. P.; Lou, S. J.; Cote, L. J.; Loser, S.; Kadleck, C. J.; Xu, T.; Szarko, J. M.; Rolczynski, B. S.; Johns, J. E.; Huang, J.; *et al.* Graphene Oxide Interlayers for Robust, High-Efficiency Organic Photovoltaics. *J. Phys. Chem. Lett.* **2011**, *2*, 3006–3012.
17. Tung, V. C.; Kim, J.; Huang, J. Graphene Oxide:Single-Walled Carbon Nanotube-Based Interfacial Layer for All-Solution-Processed Multijunction Solar Cells in Both Regular and Inverted Geometries. *Adv. Energy Mater.* **2012**, *2*, 299–303.
18. Eda, G.; Lin, Y.-Y.; Mattevi, C.; Yamaguchi, H.; Chen, H.-A.; Chen, I.-S.; Chen, C.-W.; Chhowalla, M. Blue Photoluminescence from Chemically Derived Graphene Oxide. *Adv. Mater.* **2010**, *22*, 505–509.
19. Chien, C.-T.; Li, S.-S.; Lai, W.-J.; Yeh, Y.-C.; Chen, H.-A.; Chen, I.-S.; Chen, L.-C.; Chen, K.-H.; Nemoto, T.; Isoda, S.; *et al.* Tunable Photoluminescence from Graphene Oxide. *Angew. Chem., Int. Ed.* **2012**, *51*, 6662–6666.
20. Mattevi, C.; Eda, G.; Agnoli, S.; Miller, S.; Mkhoyan, K. A.; Celik, O.; Mastrogiovanni, D.; Granozzi, G.; Garfunkel, E.; Chhowalla, M. Evolution of Electrical, Chemical, and Structural Properties of Transparent and Conducting Chemically Derived Graphene Thin Films. *Adv. Funct. Mater.* **2009**, *19*, 2577–2583.
21. Ruoff, R. Graphene: Calling all Chemists. *Nat. Nanotechnol.* **2008**, *3*, 10–11.
22. Eda, G.; Chhowalla, M. Chemically Derived Graphene Oxide: Towards Large-Area Thin-Film Electronics and Optoelectronics. *Adv. Mater.* **2010**, *22*, 2392–2415.
23. Loh, K. P.; Bao, Q.; Eda, G.; Chhowalla, M. Graphene Oxide as a Chemically Tunable Platform for Optical Applications. *Nat. Chem.* **2010**, *2*, 1015–1024.
24. Bagri, A.; Mattevi, C.; Acik, M.; Chabal, Y. J.; Chhowalla, M.; Shenoy, V. B. Structural Evolution during the Reduction of Chemically Derived Graphene Oxide. *Nat. Chem.* **2010**, *2*, 581–587.
25. Yan, J.-A.; Xian, L.; Chou, M. Y. Structural and Electronic Properties of Oxidized Graphene. *Phys. Rev. Lett.* **2009**, *103*, 086802.
26. Johari, P.; Shenoy, V. B. Modulating Optical Properties of Graphene Oxide: Role of Prominent Functional Groups. *ACS Nano* **2011**, *5*, 7640–7647.
27. Boukhvalov, D. W.; Katsnelson, M. I. Modeling of Graphite Oxide. *J. Am. Chem. Soc.* **2008**, *130*, 10697–10701.
28. Wang, L.; Sun, Y.; Lee, K.; West, D.; Chen, Z.; Zhao, J.; Zhang, S. Stability of Graphene Oxide Phases from First-Principles Calculations. *Phys. Rev. B* **2010**, *82*, 2–5.
29. Gao, W.; Alemany, L. B.; Ci, L.; Ajayan, P. M. New Insights into the Structure and Reduction of Graphite Oxide. *Nat. Chem.* **2009**, *1*, 403–408.
30. Pentcheva, R.; Wendler, F.; Meyerheim, H. L.; Moritz, W.; Jedrecy, N.; Scheffler, M. Jahn-Teller Stabilization of a "Polar" Metal Oxide Surface: Fe_3O_4(001). *Phys. Rev. Lett.* **2005**, *94*, 126101.
31. Szabo, T.; Berkesi, O.; Forgo, P.; Josepovits, K.; Sanakis, Y.; Petridis, D.; Dekany, I. Evolution of Surface Functional Groups in a Series of Progressively Oxidized Graphite Oxides. *Chem. Mater.* **2006**, *18*, 2740–2749.
32. Hunt, A.; Dikin, D. A.; Kurmaev, E. Z.; Boyko, T. D.; Bazylewski, P.; Chang, G. S.; Moewes, A. Epoxide Speciation and Functional Group Distribution in Graphene Oxide Paper-like Materials. *Adv. Funct. Mater.* **2012**, *22*, 3950–3957.
33. Kim, S.; Zhou, S.; Hu, Y.; Acik, M.; Chabal, Y. J.; Berger, C.; De Heer, W.; Bongiorno, A.; Riedo, E. Room-Temperature Metastability of Multilayer Graphene Oxide Films. *Nat. Mater.* **2012**, *11*, 544–549.
34. Zan, R.; Ramasse, Q. M.; Bangert, U.; Novoselov, K. S. Graphene Reknits Its Holes. *Nano Lett.* **2012**, *12*, 3936–3940.
35. Yin, Z.; Sun, S.; Salim, T.; Wu, S.; Huang, X.; He, Q.; Lam, Y. M.; Zhang, H. Organic Photovoltaic Devices Using Highly Flexible Reduced Graphene Oxide Films as Transparent Electrodes. *ACS Nano* **2010**, *4*, 5263–5268.
36. Tung, V. C.; Huang, J.-H.; Tevis, I.; Kim, F.; Kim, J.; Chu, C.-W.; Stupp, S. I.; Huang, J. Surfactant-Free Water-Processable Photoconductive All-Carbon Composite. *J. Am. Chem. Soc.* **2011**, *133*, 4940–4947.
37. Yun, J.-M.; Yeo, J.-S.; Kim, J.; Jeong, H.-G.; Kim, D.-Y.; Noh, Y.-J.; Kim, S.-S.; Ku, B.-C.; Na, S.-I. Solution-Processable Reduced Graphene Oxide as a Novel Alternative to PEDOT:PSS Hole Transport Layers for Highly Efficient and Stable Polymer Solar Cells. *Adv. Mater.* **2011**, *23*, 4923–4928.
38. Hossain, Z.; Johns, J. E.; Bevan, K. H.; Karmel, H. J.; Liang, Y. T.; Yoshimoto, S.; Mukai, K.; Koitaya, T.; Yoshinobu, J.; Kawai, M.; *et al.* Chemically Homogeneous and Thermally Reversible Oxidation of Epitaxial Graphene. *Nat. Chem.* **2012**, *4*, 305–309.

39. Plimpton, S. Fast Parallel Algorithms for Short-Range Molecular Dynamics. *J. Comput. Phys.* **1995**, *117*, 1–19.
40. Van Duin, A. C. T.; Dasgupta, S.; Lorant, F.; Goddard, W. A. ReaxFF: A Reactive Force Field for Hydrocarbons. *J. Phys. Chem. A* **2001**, *105*, 9396–9409.
41. Paci, J. T.; Belytschko, T.; Schatz, G. C. Computational Studies of the Structure, Behavior upon Heating, and Mechanical Properties of Graphite Oxide. *J. Phys. Chem. B* **2007**, *111*, 18099–18111.
42. Kresse, G.; Furthmuller, J. Efficient Iterative Schemes for ab-Initio Total-Energy Calculations Using a Plane-Wave Basis Set. *Phys. Rev. B* **1996**, *54*, 11169–11186.
43. Kresse, G. Efficiency of ab-Initio Total Energy Calculations for Metals and Semiconductors Using a Plane-Wave Basis Set. *Comput. Mater. Sci.* **1996**, *6*, 15–50.
44. Kresse, G.; Joubert, D. From Ultrasoft Pseudopotentials to the Projector Augmented-Wave Method. *Phys. Rev. B* **1999**, *59*, 1758.
45. Perdew, J.; Burke, K.; Ernzerhof, M. Generalized Gradient Approximation Made Simple. *Phys. Rev. Lett.* **1996**, *77*, 3865–3868.